

<https://doi.org/10.1038/s42005-025-02367-9>

Revealing the electronic structure of the current-induced metastable state in 1T-TaS₂

Check for updates

Maximilian Huber¹, Summer Zuber^{1,2}, Valeria Rosa-Rocha^{1,2}, Shannon C. Haley^{1,2}, Nicholas Dale^{1,2}, Luca Moreschini¹, Dung-Hai Lee^{1,2}, Aaron Bostwick³, Chris Jozwiak³, James G. Analytis^{1,2} & Alessandra Lanzara^{1,2,4} ✉

Among the key features for next-generation memory devices is the need for high-contrast switching between metallic and insulating states with fast switching speed and long lifetime. However, materials exhibiting such properties are rare, and their electronic structure is often poorly understood. Here, by combining state-of-the-art devices with angle-resolved photoemission spectroscopy, we study the emergence of a metastable metallic state from the insulating ground state in the charge-density wave (CDW) material 1T-TaS₂ after applying short current pulses. Analysis of the electronic structure suggests a picture in which 1T-TaS₂ transforms from a band insulator in the commensurate CDW ground state to a correlated metal in the metastable state. Moreover, the optically induced metastable state reveals a strong similarity to the current-induced one. This work provides an extensive characterization of metastable order in 1T-TaS₂ and proves how studying electronic properties under in-operando conditions is a critical step for next-generation devices.

Progress in technology relies largely on a new generation of materials with switchable properties. In particular, new forms of memory elements are needed for information technology to surpass the limitations of the current von Neumann-based computer architectures¹. Optically induced switching has driven interest in numerous material systems, as insulator-to-metal transitions in correlated materials can be driven on the ultrafast timescale and non-equilibrium states with exotic properties can be accessed^{2–6}. Integrating optical excitation mechanisms into real devices, however, is technologically challenging, driving interest in current and voltage-driven transitions in materials. Indeed, so-called resistive switching in Mott insulators and metal oxide thin films is subject to intense research, where consistent switching for millions of cycles is possible⁷. Nevertheless, fundamental aspects of the current-induced switching mechanism remain unclear, and the transitions are volatile in most cases. An exception is the prototypical charge density wave (CDW) material 1T-TaS₂, where current or voltage pulses can switch the insulating ground state into a long-lived metastable metallic state at sufficiently low temperatures^{8,9}. Optical excitation can also induce a similar metallic transition^{6,10}, prompting questions about the relationship between current and laser excitations and their resulting states. This material raises high hopes for technological applications^{11–14} and to find general characteristics that enable the discovery

of similar metastable order in other systems. A key element in understanding the nature of the metastable state in 1T-TaS₂ is its electronic band structure, which can be directly accessed using angular resolved photoemission spectroscopy (ARPES). However, such experiments are complex and require devices sufficiently small to run pulses with high current density while still being cleavable to create a clean surface. As a result, there is still only limited knowledge about the metastable state's electronic structure.

In this ARPES work, using a small beamspot and tailored samples in device geometries, we present an extensive characterization in momentum space of the current-induced metastable state in 1T-TaS₂. We find that compared to the commensurate CDW (CCDW) ground state, the band structure is modified through the whole Brillouin zone with suppressed CDW gap and CDW superlattice features, which indicates that the in-plane CDW long-range order is reduced. Most notably, a weakly dispersing band at the Fermi level appears. The metastable state is also distinct from the next metallic phase in the equilibrium phase diagram, the triclinic CDW (TCDW) phase, which shows further band shifts and a stronger reduction of the CDW amplitude. Lastly, we compare the current-induced with the light-induced metastable state and find strong similarities in the band structure. This suggests that, despite likely

¹Materials Science Division, Lawrence Berkeley National Laboratory, Berkeley, CA, USA. ²Physics Department, University of California Berkeley, Berkeley, CA, USA. ³Advanced Light Source, Lawrence Berkeley National Laboratory, Berkeley, CA, USA. ⁴Kavli Energy NanoScience Institute, Berkeley, CA, USA.

✉ e-mail: alanzara@lbl.gov

proceeding through distinct driving mechanisms, on average, both states are almost indistinguishable from an electronic structure perspective.

Results

Figure 1a shows the schematic illustration of the experimental setup: A thin flake of 1T-TaS₂ (90 μm wide and roughly 4–6 μm thick) is cut into a rectangular shape using focused ion beam fabrication (FIB) and is mounted on a sapphire plate. Silver contacts are attached to opposite ends, through which square-shaped current pulses (105 mA amplitude and 10 ms duration) are applied using a Keithley 6621 programmable current source. The experimental setup allows for simultaneous measurement of the change in transport (through the same contacts) and in the electronic structure by ARPES.

Panels b and c show the real space structure of TaS₂ in the low temperature state. Here 13 adjacent Ta atoms form so-called star-of-David (SD) clusters, which in turn are arranged commensurately to form a perfectly long-range ordered ($\sqrt{13} \times \sqrt{13}$) superstructure. The commensurate superstructure breaks mirror symmetry, allowing for two degenerate orders, which are rotated by $\pm 13.9^\circ$ compared to the original lattice. Applying current or voltage pulses below 50 K can transform the sample from the insulating commensurate CDW (CCDW) into a long-lived, metastable metallic state^{8,9,14–19}. At the surface, this metallic state consists of domains with an average size of ~ 10 nm, which are locally commensurate and phase shifted with respect to each other, separated by various different kinds of domain walls^{15–18}. This is schematically illustrated in panel d, where different domains are marked in different colors. Previous studies using scanning-tunneling spectroscopy (STS) found that the commensurate clusters themselves are metallic, while domain walls can have various different properties, depending on their exact nature¹⁷.

Figure 1e shows the resistance measured across a device for different situations: In the pristine CCDW state at 12 K after cleaving the sample (I), after applying multiple 10 ms, 105 mA pulses (II) and after heating up the sample to 90 K and subsequently cooling it back down to 12 K (III). The reported values are measured under equilibrium over the course of 30 s. After applying the current pulses (II), a clear drop in resistance from ~ 650 to $\sim 250 \Omega$ is observed, indicating the formation of a metallic state in accordance with previous studies^{9,18}. Note that the absolute resistance change cannot be directly compared to those previous studies since in this experiment R has a significant contribution of contact resistances. To prove its metastable nature, we heat up the sample to 90 K and subsequently cool it back down to 12 K, which leads to a pronounced recovery of the resistance to $\sim 500 \Omega$ (III). Note that the difference in R compared to the pristine, freshly cleaved state (I) might be caused by some residual metallic areas or simply annealing of contact resistances as R is measured through the same contacts as the current pulses are supplied.

Having established that applying current pulses indeed leads to the formation of a metastable metallic state, Fig. 1f, g show the changes in the electronic band structure measured by ARPES from the area between the contacts. Specifically, we compare cuts in the k_x - k_y plane for selected binding energies in the CCDW state (panel f) and the same cuts after applying the current pulses (panel g). The reconstructed Brillouin zone (BZ) is superimposed in grey, and the unreconstructed BZ is shown in black dashed lines. The photon energy is set to 96 eV, which effectively probes the Γ - M plane in k_z . In the CCDW phase, the Fermi surface consists of weak spots derived from a Ta_{5f} band with the periodicity of the commensurate superlattice. In contrast, in the metastable state the Fermi surface is larger and consists now of a more extended star-like shape centered at Γ , in accordance with the resistance being lower (Fig. 1e). At the same time, the backfolding replicas

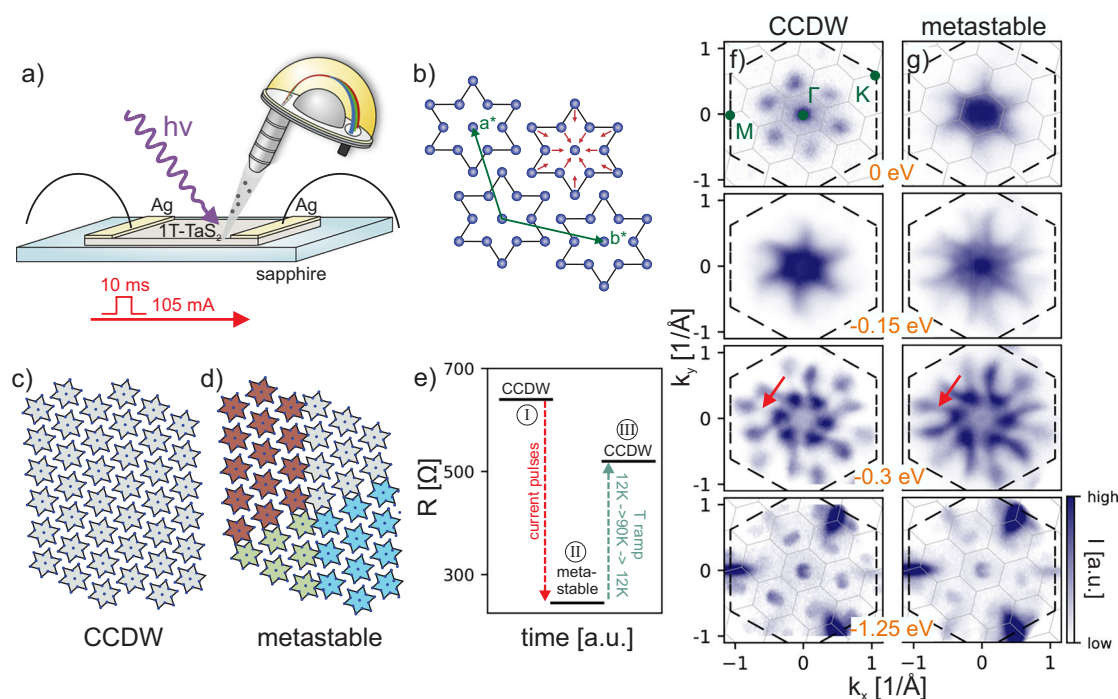


Fig. 1 | Overview of the experiment. **a** Schematic description of the experiment: A 1T-TaS₂ flake is cut into a rectangular shape and mounted on a sapphire substrate. By attaching contacts on each side one is able to apply current pulses or measure transport across the device while at the same time, the electronic structure can be probed with angle-resolved photoemission spectroscopy (ARPES). **b** Schematic illustration of the commensurate charge-density wave (CCDW) real-space structure. The star-of-David (SD) clusters are formed by 13 Ta atoms, the charge-density wave (CDW) distortion indicated by the red arrows. **c, d** Schematic cartoon of the real space structure of CCDW (**c**) and metallic mosaic state (**d**). Different colors

indicate different domains. **e** Measured resistance across the device in the pristine CCDW state at 12 K (I), after switching into the metastable state by application of multiple current pulses (II) as well as after heating to 90 K and cooling back down to 12 K (III). **f, g** Constant energy contours in the k_x - k_y plane for different binding energies in the CCDW (**f**) and the metastable (**g**) state, respectively. The Brillouin zone (BZ) of the unreconstructed normal state, as well as the CCDW state, is superimposed in black and gray lines, respectively. High symmetry points of the normal state BZ zone are indicated in green. Exemplary momentum region of a CCDW-induced gap is highlighted by red arrows.

associated with the $(\sqrt{13} \times \sqrt{13})$ reconstruction are not clearly visible anymore.

As can be seen in the second row, the shape of the metastable state at the Fermi level is very similar to the constant energy contour of the CCDW state at -0.15 eV. A full analysis of the constant-energy maps reveals that changes in the band structure are not limited to states close to the Fermi level, and clear differences, mostly in the form of a weakening of the CCDW reconstruction features, can be observed for all binding energies. For instance, at -0.3 eV gap formation due to the CCDW superlattice causes the elliptical pockets to be broken into multiple sub-manifolds, which become more connected in the metastable state (compare, for instance, the region marked by the red arrow). This indicates a weakening of the band reconstruction, suggestive of a breaking of the CCDW long-range order. Accordingly, at -1.25 eV the sulfur-derived folded bands oriented along the CCDW superlattice (indicated in grey lines) become less intense. Nonetheless, they are still visible and stay at the same position, indicating that the system preserves its overall orientation.

Overall, the changes observed in the constant energy contours suggest that the current pulses transform the system into a metallic state, stable and long-lived at low temperatures, in which the CDW long-range order is suppressed, while overall the system still preserves its orientation within different domains. This is in good agreement with the mosaic-like real-space structure of the current and voltage-induced metastable state observed with scanning-tunneling microscopy (STM) (Fig. 1d and refs. 15–18).

In Fig. 2, we characterize the evolution of the band structure from the CCDW to the metastable state along Γ - M direction. First of all, we proceed with a characterization of the CDW order from the core-level peaks. The organization of the Ta atoms into a star of David clusters with inequivalent charge distribution drives an additional splitting of the Ta_{4f} core level on top of the spin-orbit splitting into $7/2$ and $5/2$ states. This splitting is thus a direct measure of the CDW amplitude^{20,21} and can be clearly seen in the core level

spectra of the CCDW (black) and metastable (blue) state in Fig. 2a (marked by the red arrow). When switching into the metastable state, the gap becomes slightly smaller (~ 60 meV), indicating a slight reduction of the average CDW amplitude within the measured surface area. Furthermore, the peaks become more asymmetric, in accordance with the sample becoming metallic²².

Panels b-k characterize the current-driven changes in the energy vs momentum spectra. In line with previous reports^{23–28}, the CCDW state (panel b) shows a weakly dispersing band centered at Γ point below the Fermi level. The gap has been attributed to a Mott gap^{29–31} and consequently, this band has been referred to as the lower Hubbard band (LHB)²³ due to its half-filling and narrow bandwidth. We follow this notation in this work, even though the Mott picture has been contested in recent experimental and theoretical work^{24,26,32–35}, instead suggesting a hybridization gap due to layer dimerization along the out-of-plane direction. The signatures of the CCDW order in the B1 and B2 bands are the two CDW gaps (Δ_{CCDW_1} and Δ_{CCDW_2}) and the folded reconstruction bands induced by the commensurate superlattice (see orange arrows in panel b). These features in the band dispersion can be better visualized from the second derivative data, shown in panel g. Here, the weak electron-like dispersion of the LHB, less visible in the raw image plot (panel b), and the reconstruction features due to the CCDW superlattice can be well discerned. Figure 2c shows the spectrum of the current-induced metallic state. Here, additional spectral weight appears at the Fermi level, effectively closing the gap so that the spectrum becomes metallic, in line with previous reports¹⁹. Furthermore, the spectrum overall broadens in energy. Figure 2d shows an image plot taken at the same position after heating the sample to 90 K, showing that the band structure reverses to the CCDW phase, with the reopening of the gap at the Fermi level.

For a direct comparison, in panels e and f we show cuts at constant momentum as a function of energy, so-called energy distribution curves

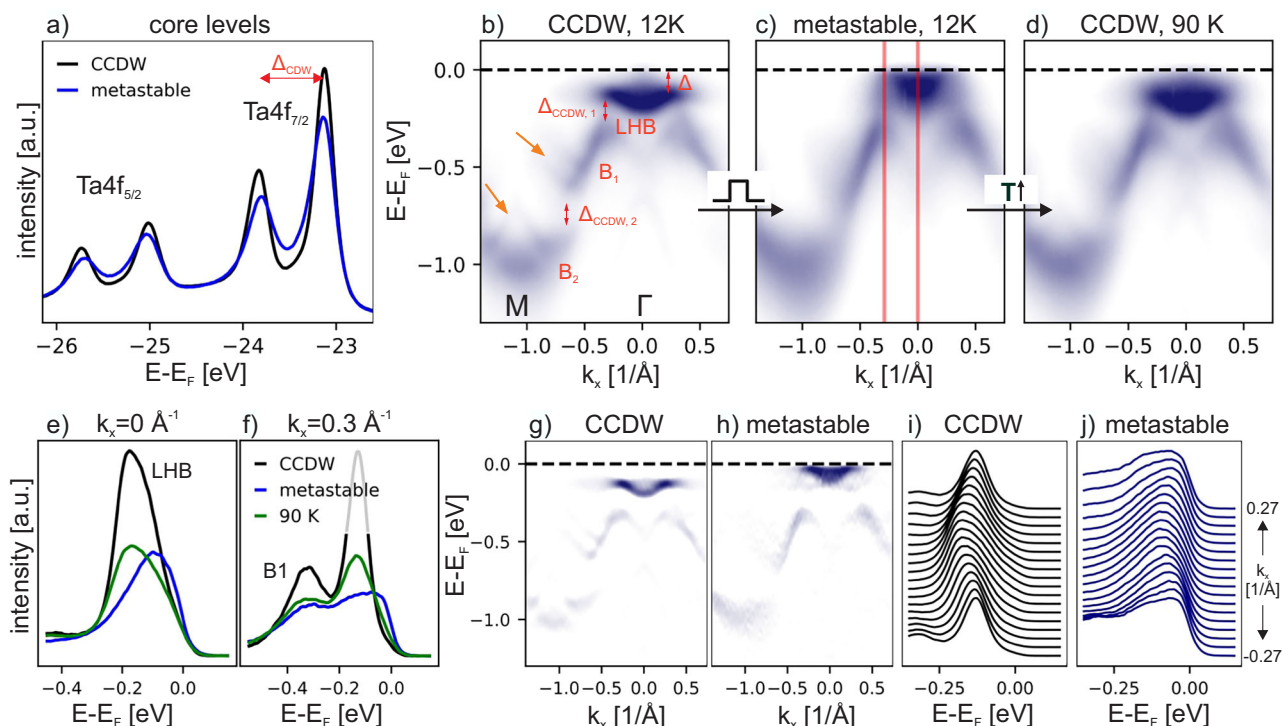


Fig. 2 | Electronic structure of the metastable state. **a** Core level spectra of 1T-TaS₂ in the CCDW (black) and metastable state (blue). **b–d** ARPES image plot along Γ - M direction in the pristine CCDW state at 12 K (**b**), in the metastable state after applying multiple current pulses (**c**), as well as after heating the metastable state to 90 K (**d**). **e** Energy distribution curves (EDCs) at Γ point for CCDW (black) and metastable (blue) state, as well as after heating to 90 K (green). Integration regions

are shown in (**c**). **f** EDCs taken at -0.3 \AA^{-1} , i.e., the region of the upper CDW gap. **g, h** Second derivative images of the CCDW (**g**) and metastable (**h**) state, respectively. To enhance visibility, images were smoothed using the Gaussian method over a window of 20 meV and 0.005 \AA^{-1} . **i, j** Stacked EDCs taken between -0.27 and 0.27 \AA^{-1} for the CCDW (**i**) and the metastable state (**j**). For clarity, all EDCs are normalized to the same height.

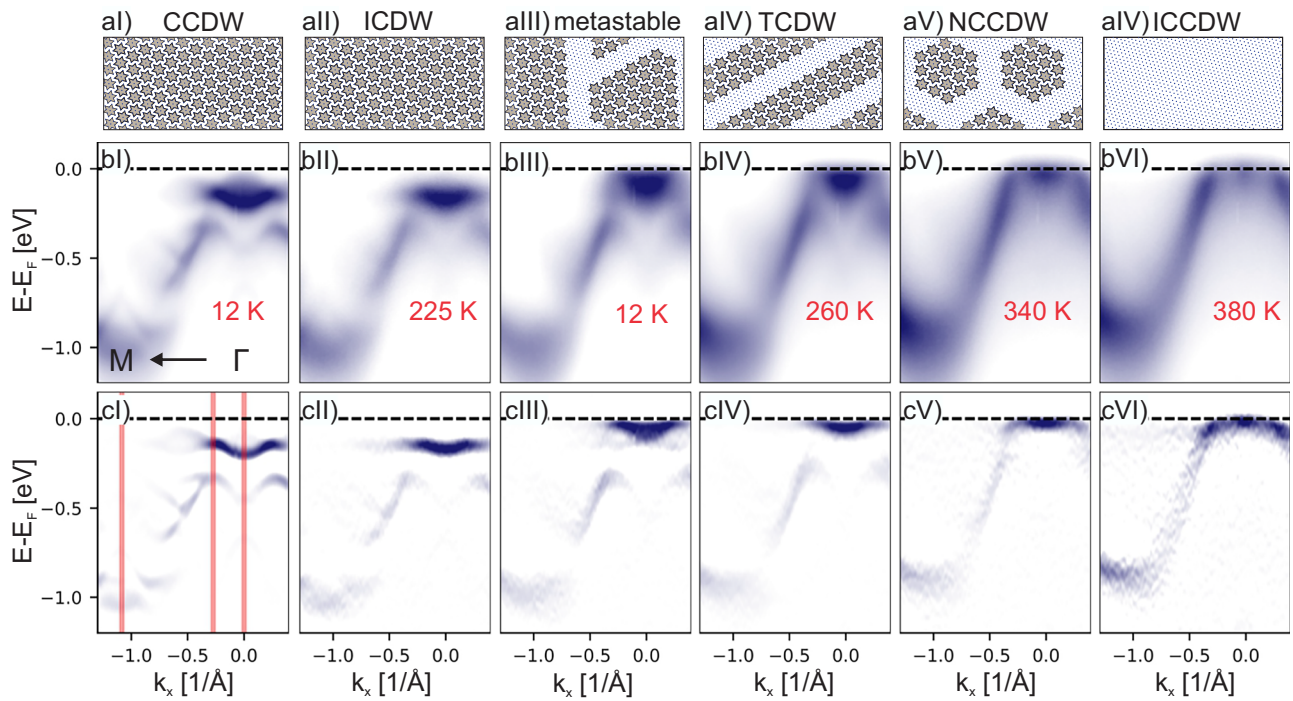


Fig. 3 | Comparison with the equilibrium high temperature phases. aI–aVI Schematic illustration of the real space structure of the surface of the metastable state as well as the equilibrium high temperature phases. For clarity, SD clusters are only shown in the commensurate domains. **bI–bVI** ARPES image plots of the metastable

state as well as the equilibrium high temperature phases along Γ - M direction. **cI–cVI** Corresponding second derivative images. To enhance visibility, images were smoothed using the Gaussian method over a window of 20 meV and 0.005 \AA^{-1} .

(EDCs) extracted from the spectra in Fig. 2b–d. The cuts are shown at the Γ point and at the momentum of the upper CDW gap, k_{CCDW_1} . Integration regions are indicated by the red lines in Fig. 2c. In the metastable state, a significant decrease in intensity of the LHB compared to the pristine CCDW state is observed. This is accompanied by a shift of the leading edge towards the Fermi level and subsequent closure of the gap, making the sample metallic. Nevertheless, in the EDC of the metastable state in Fig. 2f a weak remnant shoulder at the position of the gapped LHB at around $\sim -0.15 \text{ eV}$ can be identified, and this will be discussed in more detail later on. At the same time, the B1 band, also losing spectral weight, shifts marginally upwards, and the Δ_{CCDW_1} gap gets slightly smeared out. These effects are partially reversed at 90 K, where most notably the gap at the Fermi level opens again and the LHB increases in intensity compared to the metastable state at 12 K. The decrease of band intensities and smearing of the CDW gap in the metastable state is a sign of a reduction of the CCDW long-range order, in accordance with the changes observed along the constant energy contours in Fig. 1.

Inspection of the second derivative image of the metastable state (Fig. 2h) shows that the closing of the gap is caused by the appearance of a weakly dispersing band close to the Fermi level. To analyze the dispersion of the near- E_F states in more detail, Fig. 2i and j show stacked EDCs taken around Γ point for the CCDW (panel i) and metastable (panel j) state. For better clarity, they are normalized to the same height. In the CCDW state, the EDCs clearly show an electron-like dispersion of the LHB, as also seen in Fig. 2g. Furthermore, a weak shoulder around Γ point can be identified, likely caused by k_z broadening effects²⁴. Importantly, in the metastable state, the leading edge positions of the peaks around Γ point also show a subtle electron-like dispersion. This demonstrates that the new intensity close to the Fermi level is not caused by incoherent spectral weight filling the gap or highly localized impurity states. Previous STM/STS studies found that in the metastable state, the commensurate domains (see Fig. 1d) themselves become metallic, whereas domain walls can be both metallic and insulating, depending on their exact nature^{15–17}. As the commensurate domains cover the majority of the surface, we thus assign the in-gap state close to the Fermi

level to originate from those commensurate domains. The origin of the metallic character will be discussed in more detail later on.

1T-TaS₂ is known to undergo several first-order phase transitions as a function of temperature. When increasing the temperature starting from the CCDW phase, the commensurate order is replaced by a triclinic CDW phase (TCDW) around 240 K and subsequently into the nearly commensurate CDW (NCCDW) phase at 280 K, where hexagonal CCDW domains are separated by discommensurate areas, followed by an incommensurate CDW (ICCDW) phase at $\sim 350 \text{ K}$ ²⁴. Finally, above 550 K all CDW order is destroyed and the system becomes fully metallic. Recently, another intermediate phase (ICDW) was reported to exist in a narrow temperature range between CCDW and TCDW^{24,27,36}. This phase is characterized by a broken layer dimerization along the out-of-plane direction while the commensurate in-plane order is preserved and the surface layers remain insulating, most likely due to Mott physics. Figure 3 provides a direct comparison of the measured equilibrium band structure as a function of temperature with the metastable state. Schematic real-space structures of the surface layer are shown in panels aI–aVI, while the raw spectra along Γ - M direction are shown in panels bI–bVI and the corresponding second derivative images in panels cI–cVI. While the low temperature equilibrium commensurate charge density wave phase (CCDW) and the intermediate (ICDW) phase show highly similar dispersions besides a subtle flattening of the LHB, the evolution into the high temperature triclinic phase (TCDW) is accompanied by a closure of the gap at the Fermi level, a shift of the top of the B1 and bottom of the B2 band towards the Fermi level and the reduction of the gap between them. With increasing temperature (panels bV–bVI and cV–cVI) all gaps are almost fully closed, in accordance with previous literature^{24,25}.

Figure 3bIII and cIII show the metastable state in comparison, which by first inspection can be placed in between the ICDW and TCDW phase, with the metallic band close to the Fermi level being very similar between metastable and TCDW state, while the B1 and B2 band positions appear to be closer to the CCDW and ICDW phase.

For a more detailed comparison, in Fig. 4a–c we plot EDCs taken at Γ point, at k_{CCDW_1} and at the M point. This reproduces the impression from

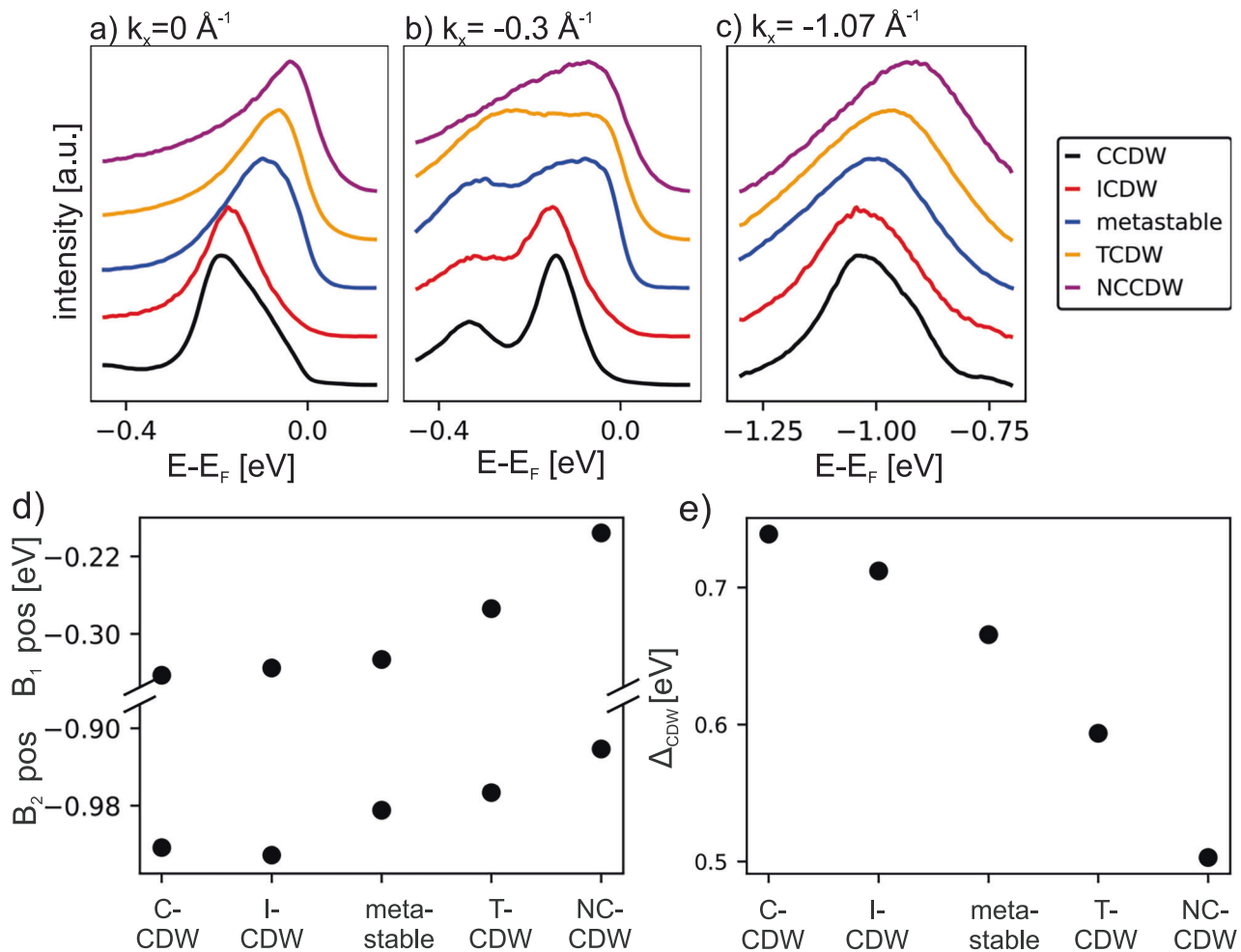


Fig. 4 | Quantitative comparison between the metastable state and the equilibrium phases. a–c EDCs at Γ (a) and -0.3 \AA^{-1} (k_{CCDW_1} , b) and M point (c) for CCDW (black), intermediate CDW (ICDW, red), metastable (blue), triclinic CDW (TCDW, orange), and the nearly-commensurate CDW phase (NCCDW, magenta).

Integration regions are shown in Fig. 3cI. For better comparison, EDCs are normalized to the same height. **d** Fitted band positions of the top of B1 band and the bottom of B2 band for the CCDW, ICDW, metastable, TCDW, and NCCDW state. **e** Core level splitting for the CCDW, ICDW, metastable, TCDW, and NCCDW state.

the second derivative images, showing that the near- E_F structure is very similar between metastable and TCDW state, both at Γ point (panel a) and k_{CCDW_1} (panel b). In contrast, the position of the top of the B1 band at k_{CCDW_1} (panel b) as well as the bottom of the B2 band at M point (panel c) are clearly shifted upwards in the TCDW phase, while for the metastable state, the band positions are closer to those of the ICDW state. For a quantitative analysis, in Fig. 4d we plot the position of the top of the B1 band as well as the bottom of the B2 band obtained from fitting the EDCs with Lorentzian peaks for the different equilibrium phases and the metastable state. The fit results show an upshift of similar magnitude for both bands in the high temperature phases, with the band positions of the metastable state lying in between ICDW and TCDW. This indicates that while the band right at the Fermi level is very similar between TCDW and the metastable state, the average CDW amplitude of the star-of-David clusters is smaller in the former. To corroborate this result, in Fig. 4e we also plot the CDW-induced core-level splitting for the different equilibrium phases and the metastable state. Results are obtained by fitting the core level spectrum with four peaks of the Doniach-Sunjić lineshape. It shows that while the gap is reduced in the metastable state compared to the pristine CCDW phase, it is still considerably larger than in the TCDW phase.

This direct comparison of the equilibrium phases with the metastable state places the latter in a special position between ICDW and TCDW. While the metallic band at the Fermi level looks very similar to the one in the TCDW, band shifts of the B1 and B2 bands, as well as the CDW amplitude obtained from the core level splitting lie in between ICDW and TCDW

states. Comparison with STM studies suggests a similar assignment with respect to the real-space structure. Indeed, the average size of the commensurate domains in the metastable state is about 100 \AA ^{15,16}, which is larger than in the TCDW phase, showing commensurate stripes with a width of $\sim 70 \text{ \AA}$ ³⁷ or the NCCDW phase with a commensurate hexagonal cluster of $\sim 70 \text{ \AA}$ diameter^{38,39}. As such, the ratio of surface area covered by commensurate domains with large CDW amplitude relative to the area covered by discommensurations with reduced CDW amplitude is larger in the metastable state than for the TCDW or NCCDW phase. To a first degree this can explain why in the metastable state the average CDW gap size is smaller than in the TCDW phase while the weakly dispersing band close to the Fermi level, likely originating from the commensurate clusters, is very similar.

The appearance of a metastable metallic state in 1T-TaS₂ was first reported by using ultrashort optical laser pulses⁶, displaying overall transport properties similar to the current-driven metastable state⁸. This prompts the question of how the two states are related. In Fig. 5 we compare the current (top row) with the light-induced (bottom row) metastable state by comparing second derivative images of the ARPES spectra as well as EDCs at Γ point and k_{CCDW_1} . The insets show schematic illustrations of the experiment for switching by current pulses and a single laser pulse, respectively. Experimental details can be found in the method section. Despite the two states being obtained through different mechanisms, the data clearly shows that besides slight variations (note that both experiments were done on different samples at different endstations, for details see the

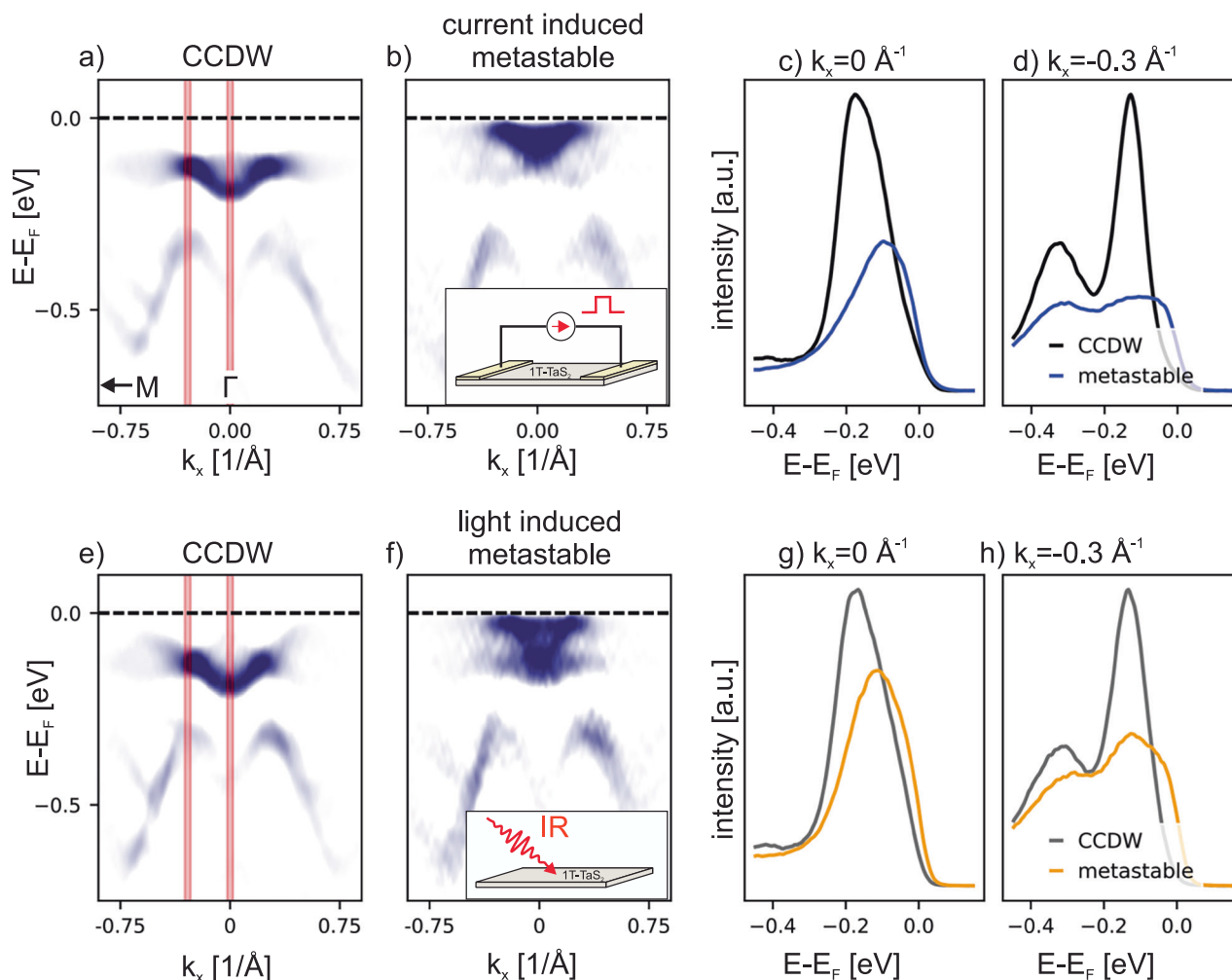


Fig. 5 | Comparison between current- and light-induced metastable state. **a** Second derivative image of the CCDW state along Γ - M direction. **b** Second derivative image of current-induced metastable state. **c, d** EDCs at Γ (**c**) and

-0.3\AA^{-1} (**d**) for CCDW (black) and current-induced metastable (blue) state (integration regions shown as inset in **a**). **e-h** Corresponding plots to **a-d** but for the light-induced metastable state.

Methods section) the changes in the band structure are qualitatively very similar, including the appearance of a weakly dispersing band at the Fermi level and a weakening of the band intensities and CCDW reconstruction features as well as slight upshift of the B1 band top.

This qualitative agreement between both metastable states is remarkable, since optical and current pulses interact with the sample in distinct ways, and the two excitation methods in the present case have characteristic parameters that differ by orders of magnitude. For instance, the pulse length of the laser is 150 fs compared to 10 ms for the current pulse. These differences likely lead to different switching mechanisms, which are in both cases still debated. While previous STM studies reported subtle differences in the real-space domain structure between the two excitation methods^{17,40}, a recent diffraction study found that both light and current-induced metastable states are structurally equivalent⁴¹. This is in line with our ARPES results, showing the same characteristic changes in the band structure for both metastable states. The different switching methods could potentially lead to slightly different domain sizes with different discommensuration networks, which might lead to subtle variations in near- E_F states, however further experiments are necessary to allow for such a detailed comparison.

Discussion

The similarity between light and current-induced metastable states indicates the presence of a local minimum of the free energy landscape in which the system can be trapped by any sufficiently fast excitation, irrespective of the

exact mechanistic pathway. Once the system becomes locked in this state due to an initial condition or an external driving force, it requires a long time to transition out of it.

From an electronic structure perspective, the metastable state is characterized by an in-gap weakly dispersing band close to the Fermi level. This is accompanied by a weakening of the superlattice features, indicating a reduction of long-range order and the average CDW amplitude. These observations agree well with a real-space picture in which commensurate clusters, most likely causing the in-gap state, are separated by discommensuration networks.

As discussed previously, recent literature agrees that the gap at the Fermi level in the CCDW ground state is a hybridization gap caused by layer dimerization along the out-of-plane direction^{32,34}. Even though this order has been shown to be broken in both current and optical induced metastable state^{19,41,42}, it is questionable if that alone is sufficient to make the sample surface metallic. Indeed, a number of studies^{24,32,33} showed that even isolated TaS₂ layers on the surface are still gapped, likely due to Mott physics. This can be directly seen in the form of the ICDW phase (Fig. 3aII, bII, cII), in which the ARPES spectra show a clear gap at the Fermi level, while the bilayer hybridization is broken²⁴. Therefore, it is likely that at least for the sample surface the reduction of the in-plane long-range order, indicated by the weakening of superlattice features and reduction of the CDW gaps, is an important ingredient in making the sample metallic in addition to the changes along the out-of-plane direction. In particular, the spectral weight transfer from the LHB into the in-gap state close to the Fermi level is

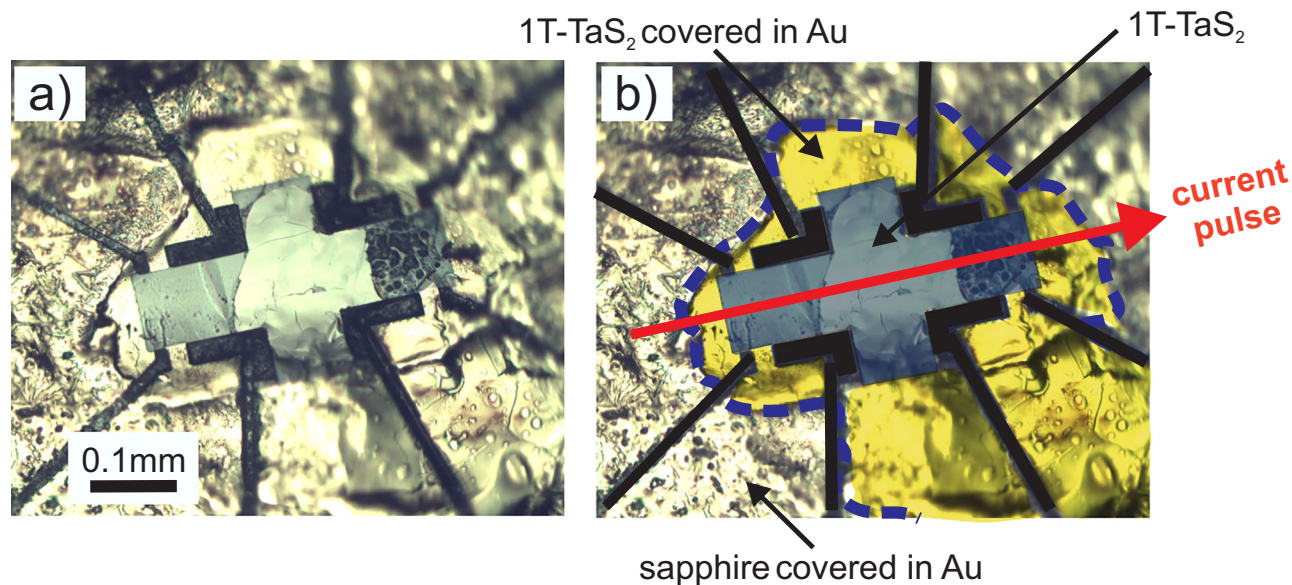


Fig. 6 | Layout of the device. **a** Microscope image of a cleaved sample taken after an experiment. **b** Same as **a** but with different areas marked in different colors. Dotted blue line marks the outline of the 1T-TaS₂ flake; yellow regions are where the flake is covered in gold, while in blue regions the gold was milled away from the TaS₂ surface.

Black lines are areas where the gold and 1T-TaS₂ was fully removed using FIB to create well-defined current paths. The region outside of the flake is sapphire-covered in gold. The red arrow indicates the main pulsing direction through which current pulses are applied and resistance is measured.

reminiscent of the closing of a Mott gap^{43,44}, possibly caused by the reduction of CDW amplitude¹⁶, a change of local stacking order effectively modifying the out-of-plane hopping term¹⁵, screening by domain walls⁴⁵ or disorder. The remnant LHB could in principle, also originate from small areas inside the clusters that are locally still gapped, which have indeed been found in previous STM/STS studies¹⁵. However, their occurrence has been described as very rare, while in the ARPES data, the intensity of the remnant LHB is roughly 25% of the peak amplitude of the CCDW phase. Overall, the spectral weight transfer together with the fact that all characteristic features in the band structure of the metastable state lie in between the Mott insulating ICDW phase and the metallic TCDW phase support the notion that 1T-TaS₂ transforms from a band insulator in the CCDW ground state into a correlated metal in the metastable state, as has been proposed in a previous STM study¹⁶.

Conclusion

In summary, using FIB-fabricated devices, we drove the formation of a metastable metallic state in 1T-TaS₂ and studied its electronic structure in operando using ARPES. The data revealed that the newly formed metallic state results from the sudden appearance of an in-gap state close to the Fermi level, accompanied by weakening of the superlattice features, indicating a reduction of long-range order, while the overall CDW amplitude gets only slightly reduced. The characterization of the temperature dependence of the band structure in different ordered states proves that the metastable state lies in between the Mott insulating ICDW and the metallic TCDW phase. This placement in the equilibrium phase diagram, together with the spectral weight transfer from the LHB into the in-gap state, suggests that the system undergoes a transition from a band insulator in the CCDW ground state to a correlated metal in the metastable state. The similarity of the electronic structure of the current- and the light-induced metastable state, despite likely proceeding through very different mechanisms, demands a better understanding of what drives metastable order. This work contributes to the understanding of metastable states in 1T-TaS₂ and related materials and helps pave the way for future adoption into devices. More in general, the proven ability to study materials' properties under in-operando conditions is a critical step for next-generation materials and technological applications.

Methods

Device fabrication

Single crystals of 1T-TaS₂ were obtained by chemical vapor transport (CVT). These were exfoliated using Nitto tape to obtain crystal flakes of about 400 × 400 μm on the surface and between 4 and 6 μm in thickness. The flake was then mounted on a sapphire substrate using Torr Seal epoxy by Agilent. After a ~200 nm thick layer of gold had been sputtered on the sample and substrate, the gold was milled away from the active area of the device using a Helios G4 focused ion beam (FIB). Furthermore, by milling the 1T-TaS₂ flake and Au layer down to the sapphire surface well-defined current pathways were created. Subsequently, the device was transferred on a chip carrier. Then contacts were attached from the side of the device to the sides of the chip carrier, which in turn is mounted to a special sample holder. In order to obtain a pristine surface for the ARPES measurement, a ceramic post of 250 μm diameter was glued on top of the active area of the device using Torr Seal. This allows for the removal of a thin top layer of the crystal under UHV by cleaving.

Figure 6a shows an optical microscope image of such a cleaved sample taken after an experiment. Figure 6b shows the same image with the different regions marked in different colors.

ARPES Measurements

ARPES experiments on the current-induced metastable state were carried out at the microARPES endstation of beamline 7.0.2.1 at the Advanced Light Source. Samples were cleaved in situ at 12 K at a base pressure of $\sim 2 \times 10^{-11}$ mbar. Current was applied through square pulses of 105 mA amplitude and 10 ms duration using a Keithley 6221. ARPES spectra of the metastable state are taken after applying 50 pulses overall. During ARPES measurements, the sample was grounded through the electrical contacts; no charging effects were observed. Transport properties were measured using a Keithley 2450 Source Measure Unit.

ARPES data on the light-induced metastable state were taken at the nanoARPES endstation of beamline 7.0.2.2. Samples were cleaved in situ at 25 K using a ceramic post. The metastable state was created by focusing a single ~20 nJ laser pulse of 800 nm wavelength and 150 fs pulse width down to ~10 μm diameter, effectively exciting the sample with 25 mJ/cm².

Data availability

The datasets generated and/or analyzed during the current study are not publicly available as they contain additional findings not reported in this manuscript, but are available from the corresponding author on reasonable request.

Received: 27 March 2025; Accepted: 12 October 2025;

Published online: 15 November 2025

References

- Wang, Z. et al. Resistive switching materials for information processing. *Nat. Rev. Mater.* **5**, 173–195 (2020).
- Torre, A. D. L. et al. Colloquium: Nonthermal pathways to ultrafast control in quantum materials. *Re. Mod. Phys.* **93**, 041002 (2021).
- Fausti, D. et al. Light-induced superconductivity in a stripe-ordered cuprate. *Science* **331**, 189–191 (2011).
- Kogar, A. et al. Light-induced charge density wave in LaTe_3 . *Nat. Phys.* **16**, 159–163 (2020).
- Huber, M. et al. Ultrafast creation of a light-induced semimetallic state in strongly excited 1T-TaS_2 . *Sci. Adv.* **10**, ead14481 (2024).
- Stojchevska, L. et al. Ultrafast switching to a stable hidden quantum state in an electronic crystal. *Science* **344**, 177–180 (2014).
- Zhou, Y. & Ramanathan, S. Mott memory and neuromorphic devices. *Proc. IEEE* **103**, 1289–1310 (2015).
- Vaskivskiy, I. et al. Controlling the metal-to-insulator relaxation of the metastable hidden quantum state in 1T-TaS_2 . *Sci. Adv.* **1**, e1500168 (2015).
- Vaskivskiy, I. et al. Fast electronic resistance switching involving hidden charge density wave states. *Nat. Commun.* **7**, 11442 (2016).
- Maklar, J. et al. Coherent light control of a metastable hidden state. *Sci. Adv.* **9**, eadi4661 (2023).
- Mraz, A. et al. Charge configuration memory devices: Energy efficiency and switching speed. *Nano Lett.* **22**, 4814–4821 (2022).
- Venturini, R. et al. Ultraefficient resistance switching between charge-ordered phases in 1T-TaS_2 with a single picosecond electrical pulse. *Appl. Phys. Lett.* **120**, 253510 (2022).
- Mihailovic, D. et al. Ultrafast non-thermal and thermal switching in charge configuration memory devices based on 1T-TaS_2 . *Appl. Phys. Lett.* **119**, 013106 (2021).
- Devidas, T. R. et al. Spontaneous conducting boundary channels in 1T-TaS_2 <https://arxiv.org/pdf/2405.02036>.
- Ma, L. et al. A metallic mosaic phase and the origin of mott-insulating state in 1T-TaS_2 . *Nat. Commun.* **7**, 10956 (2016).
- Cho, D. et al. Nanoscale manipulation of the Mott insulating state coupled to charge order in 1T-TaS_2 . *Nat. Commun.* **7**, 10453 (2016).
- Park, J. W., Lee, J. & Yeom, H. W. Zoology of domain walls in quasi-2D correlated charge density wave of 1T-TaS_2 . *npj Quantum Mater.* **6**, 32 (2021).
- Mraz, A. et al. Manipulation of fractionalized charge in the metastable topologically entangled state of a doped Wigner crystal. *Nat. Commun.* **14**, 8214 (2023).
- Nitzav, Y. et al. Emergence of a Fermi surface in the current-driven hidden state of 1T-TaS_2 . <http://arxiv.org/abs/2407.05535> (2024).
- Hellmann, S. et al. Ultrafast melting of a charge-density wave in the Mott insulator 1T-TaS_2 . *Phys. Rev. Lett.* **105**, 1–4 (2010).
- Hughes, H. P. & Pollak, R. A. Charge density waves in layered metals observed by X-ray photoemission. *Philos. Mag.* **34**, 1025–1046 (1976).
- Hüfner, S. *Photoelectron spectroscopy: principles and applications* (Springer, 2003), 3 edn.
- Sohr, C., Stange, A., Bauer, M. & Rossmagel, K. How fast can a Peierls-Mott insulator be melted? *Faraday Discuss.* **171**, 243–257 (2014).
- Wang, Y. D. et al. Band insulator to mott insulator transition in 1T-TaS_2 . *Nat. Commun.* **11**, 4215 (2020).
- Yang, H. F. et al. Visualization of chiral electronic structure and anomalous optical response in a material with chiral charge density waves. *Phys. Rev. Lett.* **129**, 156401 (2022).
- Ritschel, T., Berger, H. & Geck, J. Stacking-driven gap formation in layered 1T-TaS_2 . *Phys. Rev. B* **98**, 195134 (2018).
- Jung, J., Jin, K. H., Kim, J. & Yeom, H. W. Control over a wide phase diagram of 2d correlated electrons by surface doping; $\text{K}/1\text{T-TaS}_2$. *Nano Lett.* **23**, 8029–8034 (2023).
- Perfetti, L., Gloor, T. A., Mila, F., Berger, H. & Gioni, M. Unexpected periodicity in the quasi-two-dimensional Mott insulator 1T-TaS_2 revealed by angle-resolved photoemission. *Phys. Rev. B - Condens. Matter Mater. Phys.* **71**, 153101 (2005).
- Fazekas, P. & Tosatti, E. Electrical, structural and magnetic properties of pure and doped 1T-TaS_2 . *Philos. Mag. B* **39**, 229–244 (1979).
- Kim, J. J., Yamaguchi, W., Hasegawa, T. & Kitazawa, K. Observation of Mott localization gap using low temperature scanning tunneling spectroscopy in commensurate 1T-TaS_2 . *Phys. Rev. Lett.* **73**, 2103 (1994).
- Dardel, B. et al. Temperature-dependent pseudogap and electron localization in 1T-TaS_2 . *Phys. Rev. B* **45**, 1462 (1992).
- Butler, C. J., Yoshida, M., Hanaguri, T. & Iwasa, Y. Mottness versus unit-cell doubling as the driver of the insulating state in 1T-TaS_2 . *Nat. Commun.* **11**, 2477 (2020).
- Lee, J., Jin, K. H. & Yeom, H. W. Distinguishing a Mott insulator from a trivial insulator with atomic adsorbates. *Phys. Rev. Lett.* **126**, 196405 (2021).
- Lee, S. H., Goh, J. S. & Cho, D. Origin of the insulating phase and first-order metal-insulator transition in 1T-TaS_2 . *Phys. Rev. Lett.* **122**, 106404 (2019).
- Ritschel, T. et al. Orbital textures and charge density waves in transition metal dichalcogenides. *Nat. Phys.* **11**, 328–331 (2015).
- Dong, J. et al. Dynamics of electronic states in the insulating intermediate surface phase of 1T-TaS_2 . *Phys. Rev. B* **108**, 155145 (2023).
- Burk, B., Thomson, R. E., Clarke, J. & Zettl, A. Surface and bulk charge density wave structure in 1T-TaS_2 . *Science* **257**, 362–264 (1992).
- Wu, X. L. & Lieber, C. M. Hexagonal domain-like charge density wave phase of TaS_2 determined by scanning tunneling microscopy. *Science* **243**, 1703–1705 (1989).
- Park, J. W., Cho, G. Y., Lee, J. & Yeom, H. W. Emergent honeycomb network of topological excitations in correlated charge density wave. *Nat. Commun.* **10**, 4038 (2019).
- Gerasimenko, Y. A., Karpov, P., Vaskivskiy, I., Brazovskii, S. & Mihailovic, D. Intertwined chiral charge orders and topological stabilization of the light-induced state of a prototypical transition metal dichalcogenide. *npj Quantum Mater.* **4**, 32 (2019).
- Burri, C. et al. Non-destructive imaging of bulk electrical ‘hidden’ state switching in a 1T-TaS_2 cryo-memory device. <http://arxiv.org/abs/2411.04830> (2024).
- Stahl, Q. et al. Collapse of layer dimerization in the photo-induced hidden state of 1T-TaS_2 . *Nat. Commun.* **11**, 1247 (2020).
- Damascelli, A., Hussain, Z. & Shen, Z. X. Angle-resolved photoemission studies of the cuprate superconductors. *Rev. Mod. Phys.* **75**, 473 (2003).
- Hu, C. et al. Momentum-resolved visualization of electronic evolution in doping a mott insulator. *Nat. Commun.* **12**, 1356 (2021).
- Zwick, F. et al. Spectral consequences of broken phase coherence in 1T-TaS_2 . *Phys. Rev. Lett.* **81**, 1058 (1998).

Acknowledgements

The authors thank Cheng Hu for taking the temperature-dependent equilibrium data and for useful discussions. L.M. acknowledges helpful discussions with Alfred Zong. This work was primarily funded by the U.S. Department of Energy (DOE), Office of Science, Office of Basic Energy Sciences, Materials Sciences

and Engineering Division under contract no. DE-AC02-05CH11231 (Ultrafast Materials Science program KC2203). This research used resources of the Advanced Light Source, which is a DOE Office of Science User Facility under contract no. DE-AC02-05CH11231. The FIB and fabrication part of the process was funded by the U.S. Department of Energy (DOE), Office of Science, Office of Basic Energy Sciences, Materials Sciences and Engineering Division under contract no. DE-AC02-05CH11231 (Quantum Materials program KC2202). A.L. also acknowledges support from the Gordon and Betty Moore Foundation EPiQS Initiative through grant no. GBMF4859 for the implementation of the experimental setup.

Author contributions

A.L. and J.G.A. designed the project. Samples were fabricated by V.R.R. and S.H. Data on the current-induced metastable state were collected by M.H. with the help of L.M., N.D., C.J., and A.B. Data on the light-induced metastable state were collected by S.Z. with the help of M.H. and C.J. Data were analyzed by M.H. and discussed with all authors. D.H.L. contributed to the discussion sections. Manuscript preparation was done by M.H. with input from all co-authors.

Competing interests

The authors declare no competing interests.

Additional information

Correspondence and requests for materials should be addressed to Alessandra Lanzara.

Peer review information *Communications Physics* thanks the anonymous reviewers for their contribution to the peer review of this work.

Reprints and permissions information is available at <http://www.nature.com/reprints>

Publisher's note Springer Nature remains neutral with regard to jurisdictional claims in published maps and institutional affiliations.

Open Access This article is licensed under a Creative Commons Attribution 4.0 International License, which permits use, sharing, adaptation, distribution and reproduction in any medium or format, as long as you give appropriate credit to the original author(s) and the source, provide a link to the Creative Commons licence, and indicate if changes were made. The images or other third party material in this article are included in the article's Creative Commons licence, unless indicated otherwise in a credit line to the material. If material is not included in the article's Creative Commons licence and your intended use is not permitted by statutory regulation or exceeds the permitted use, you will need to obtain permission directly from the copyright holder. To view a copy of this licence, visit <http://creativecommons.org/licenses/by/4.0/>.

© The Author(s) 2025